

Out-of-plane stability of buckling-restrained braces including moment transfer capacity

Toru Takeuchi^{1,*}, Hitoshi Ozaki², Ryota Matsui¹ and Fatih Sutcu³

¹*Department of Architecture and Building Engineering, Tokyo Institute of Technology, Tokyo, Japan*

²*Nikken Housing System Ltd, Tokyo, Japan*

³*Department of Architecture, Istanbul Technical University, Istanbul, Turkey*

SUMMARY

Buckling-restrained braces (BRBs) are widely used as ductile seismic-resistant and energy-dissipating structural members in seismic regions. Although BRBs are expected to exhibit stable hysteresis under cyclic axial loading, one of the key limit states is global flexural buckling, which can produce an undesirable response. Many prior studies have indicated the possibility of global buckling of a BRB before its core yields owing to connection failure. In this paper, BRB stability concepts are presented, including their bending-moment transfer capacity at restrainer ends for various connection stiffness values with initial out-of-plane drifts, and a unified simple equation set for ensuring BRB stability is proposed. Moreover, a series of cyclic loading tests with initial out-of-plane drifts are conducted, and the results are compared with those of the proposed equations. © 2013 The Authors. *Earthquake Engineering & Structural Dynamics* published by John Wiley & Sons Ltd.

Received 13 July 2013; Revised 4 September 2013; Accepted 5 September 2013

KEY WORDS: buckling-restrained brace; connections; cyclic loading test; buckling; moment transfer capacity; stability concepts

1. INTRODUCTION

Buckling-restrained braces (BRBs) are expected to exhibit stable hysteresis when subjected to in-plane cyclic axial loading, as described in seismic provisions as AIJ 2009 [1] and AISC 341–10 [2]. As determined in these provisions, various conditions are required to ensure the stable BRB hysteresis. Takeuchi *et al.* investigated the relation between the cumulative deformation capacity and the applied loading history [3] of a BRB and discussed the influence of local buckling on BRB strength and ductility [4]. Furthermore, several past studies have highlighted the risk of global BRB buckling induced by connection failure such as plastic hinges introduced at connection zone prior to core yielding (Figure 1). For instance, Tsai *et al.* [5] and Lin *et al.* [6] reported the phenomenon of global buckling related to connection failure in BRB frame tests, and Wigle *et al.* [7] discussed the effect of connections on BRB performance. Koetaka *et al.* [8] discussed the conditions leading to instability, under which bending-moment transfer capacity at the restrainer ends is lost and gusset plates are designed to be rotationally rigid. Zao *et al.* [9, 10] investigated the stability conditions of BRBs with pin-ended connections. Hikino *et al.* [11] carried out shaking table tests on BRB frames, and Okazaki *et al.* [12] suggested stiffness requirements for gusset plates under one-sided buckling considering the loss of restrainer moment transfer capacity and confirmed the requirements by the test results. In

*Correspondence to: Toru Takeuchi, Department of Architecture and Building Engineering, Tokyo Institute of Technology, Tokyo, Japan.

†E-mail: ttoru@arch.titech.ac.jp

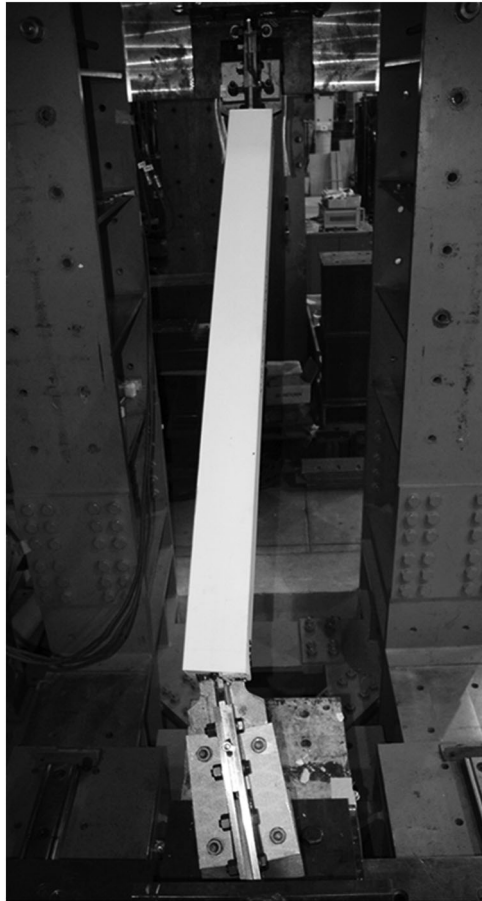


Figure 1. Global buckling of buckling-restrained brace including connections (MRL 1.0S2 in Table IV).

addition, the stiffness and strength requirements at connections have also been investigated through several other BRB frame tests [13–17].

However, in previous studies, stability concepts including the effects of bending-moment transfer capacity at the restrainer ends for varying rotational stiffness values of the gusset plates have not yet been clarified. The effect of story drift in the out-of-plane direction for simulating the transverse component of ground motion was not considered either. In this paper, the stability requirements for BRBs including the aforementioned conditions are discussed, and a simple set of equations covering these conditions is proposed. In addition, cyclic axial loading tests of BRBs with initial out-of-plane drift are performed, and the accuracy of the proposed equation set is verified.

2. STABILITY CONDITION FOR BRBS INCLUDING CONNECTIONS

In AIJ Recommendations for Stability Design of Steel Structures [1], the implementation of the following two concepts is presented for preventing global instability as shown in Figure 2.

Concept (1): Although plastic hinges without bending-moment transfer capacity is allowed at the restrainer ends, the stability conditions are satisfied individually for the restrained zone and the connection zone [Figure 2(a)].

Concept (2): When bending-moment transfer capacity is provided at the restrainer ends, the composite stability of the restrained zone and the connection zone are ensured [Figure 2(b)].

For Concept (1), the following equations were proposed by Koetaka *et al.* [8].

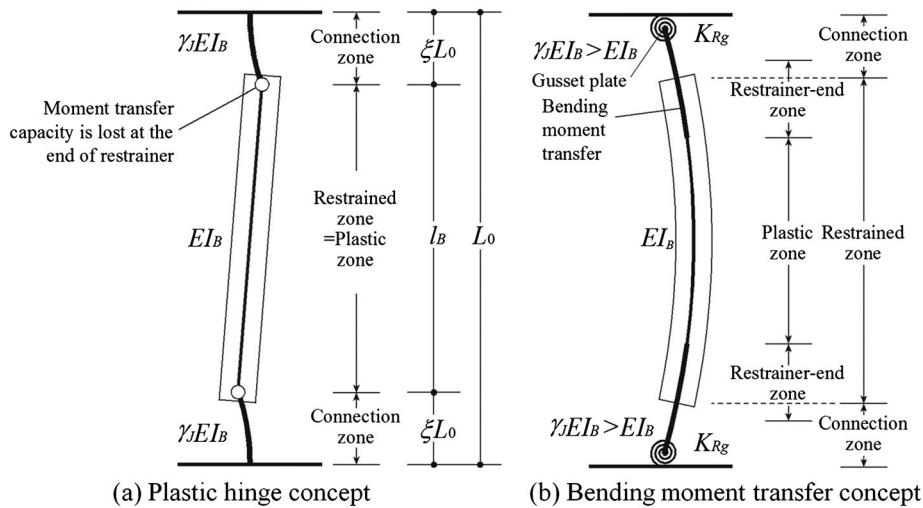


Figure 2. Buckling-restrained brace stability condition concepts (AIJ Recommendations for Stability Design of Steel Structures, 2009).

The stability condition of the restrained zone:

$$M_y^B \geq \frac{(a + e + s_r)N_{cu}}{1 - N_{cu}/N_{cr}^R} \tag{1}$$

The stability condition of the connection zone:

$$\frac{(1 - 2\xi)\pi^2\gamma_J EI_B}{(2\xi L_0)^2} > N_{cu} \tag{2}$$

where M_y^B denotes yield bending strength of the restrainer, a denotes maximum imperfection along the restrainer, e denotes axial force eccentricity, s_r denotes the core–restrainer clearance, N_{cu} denotes the maximum axial strength of the core plates, normally estimated as 1.2–1.5 times the yield strength of the core plates, including hardening, N_{cr}^R denotes the Euler buckling strength of the restrainer, $\gamma_J EI_B$ denotes the bending stiffness of the connections, L_0 denotes the total BRB length, and ξL_0 denotes the connection zone length.

Equation (2) is based on the assumption that the ends of the connection zones are rigidly fixed against rotation; in practice, however, substantially stiff gusset plates are required to satisfy this condition (e.g., stiffened gusset plates similar to the one shown in Figure 3(c)). Moreover, rotation of the beam to which BRBs are connected should be prevented using stiff secondary beams.

For Concept (2), Matsui *et al.* [17] indicated that the restrainer-end zone can transfer bending moment as large as the smaller of the bending strength of the restrainer or the neck, if the extension of the insert zone L_{in} into the restrainer is more than the width of the core plate (Figure 4). In Figure 4, the neck represents the portion of the cruciform sectioned core that extends beyond the

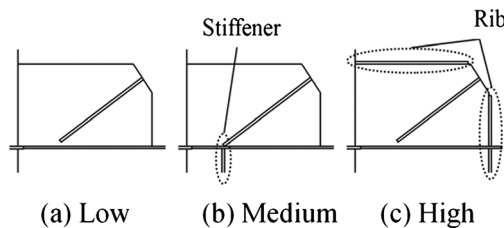


Figure 3. Connection with varying stiffness.

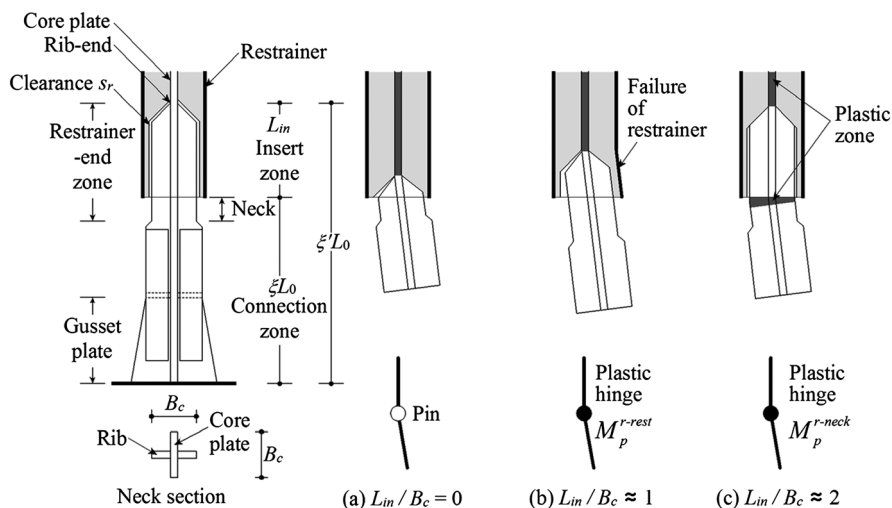


Figure 4. Bending moment transfer at restrainer ends.

restrainer case. When the rotational stiffness of the gusset plate is relatively low as in Figure 3(a), the core–restrainer clearance generates an initial imperfection that can be assumed as $a_r = a + e + s_r + (2s_r/L_{in})\xi L_0$, as shown in Figure 5. Then, the relationship between the axial force N , and out-of-plane deformations y_r at the end of the restrainer can be approximated by the following equation (Figure 6).

$$N = \frac{y_r}{y_r + a_r} N_{cr}^B \tag{3}$$

where N_{cr}^B denotes the global elastic buckling strength of BRB, including the effects of the connection zone’s bending stiffness, and the gusset plates’ rotational stiffness. In Figure 6, the axial force approaches N_{cr}^B asymptotically for increasing values of y_r ; however, the elastic buckling process is interrupted when the brace reaches its ultimate strength as computed by collapse mechanisms resulting from the plasticity at the restrainer ends. The intersection point of the elastic buckling path and the ultimate strength path is defined as the stability limit. In cases where the maximum axial strength of the core, N_{cus} is lower than the stability limit, the brace is considered stable, and the BRB core exhibits

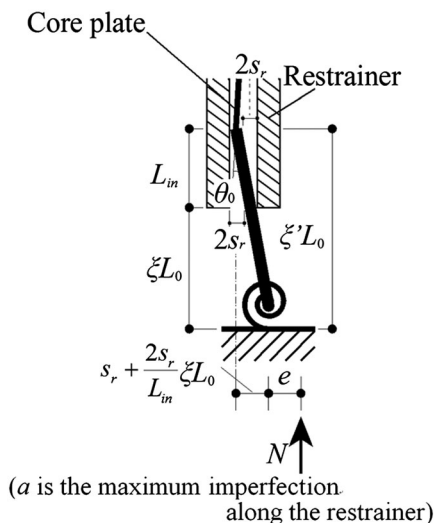


Figure 5. Assumed initial imperfection.

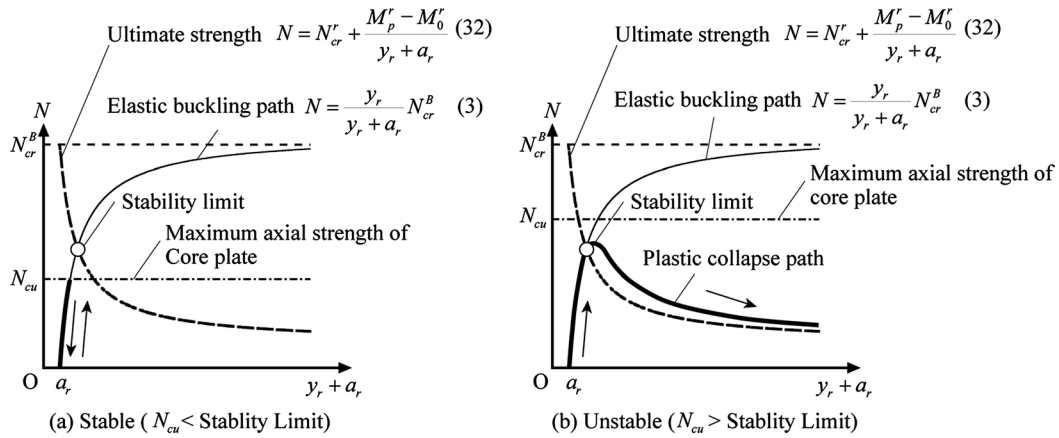


Figure 6. Buckling-restrained brace stability concepts and limits.

regular hysteretic behavior. However, when N_{cu} exceeds the stability limit, the plastic hinges are produced at the insert zone, and the hysteretic behavior is considered to be interrupted by the global buckling collapse mechanisms.

The ultimate strength values of the possible collapse mechanisms are estimated using the models shown in Figure 7. As can be seen in this figure, the BRB is modeled with rotational springs of stiffness K_{Rg} at both gusset plates. Then, an initial imperfection a_r is modeled at restrainer ends. When the bending moment at the restrainer-end zone exceeds the restrainer moment transfer capacity M_p^r , the load on the BRB exceeds its ultimate strength, eventually resulting in buckling.

Firstly, the gusset plates are assumed to be rigid ($K_{Rg} \rightarrow \infty$), and out-of-plane deformations of the connection zone during the mechanism phase are assumed to be of sinusoidal shape, as shown in Figure 7(a) and given in Equation (4).

$$y = \frac{a_r x}{\xi L_0} + y_r \left[1 - \cos\left(\frac{\pi x}{2\xi L_0}\right) \right] \quad (4)$$

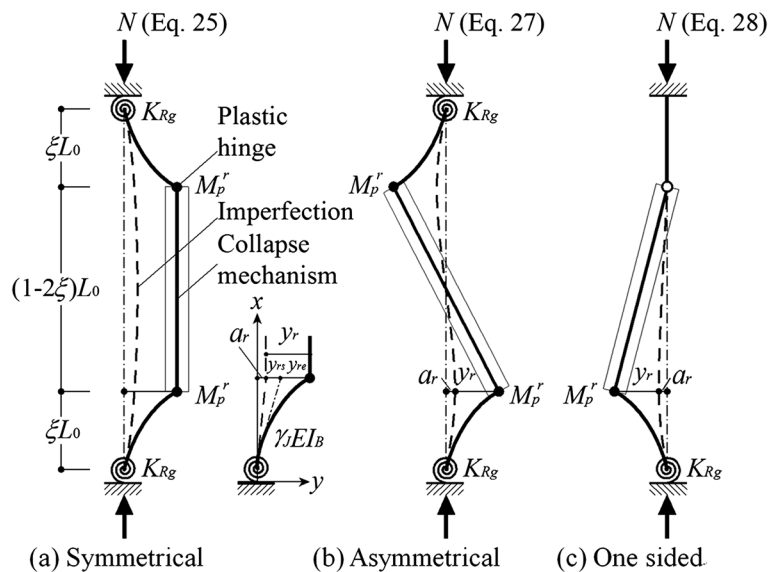


Figure 7. Collapse mechanisms with rotational springs at gusset plates.

Then, the strain energy stored in both connection zones is given as follows:

$$U_\varepsilon = 2 \int_0^{\xi L_0} \frac{\gamma_J EI_B}{2} \left(\frac{d^2}{dx^2} \left(y - \frac{a_r}{\xi L_0} \right) \right)^2 dx = \frac{\pi^4 \gamma_J EI_B y_r^2}{32 (\xi L_0)^3} \quad (5)$$

The rotation angle of the plastic hinges is expressed as follows:

$$\Delta\theta_r = \frac{dy}{dx} \Big|_{x=\xi L_0} - \frac{a_r}{\xi L_0} = \frac{\pi}{2\xi L_0} y_r \quad (6)$$

Then, the plastic strain energy stored in the plastic hinges is as follows:

$$U_p = 2M_p^r \Delta\theta_r = \frac{\pi y_r}{\xi L_0} M_p^r \quad (7)$$

The axial deformation is as follows:

$$\Delta u_g = 2 \cdot \frac{1}{2} \int_0^{\xi L_0} \left[\left(\frac{dy}{dx} \right)^2 - \left(\frac{a_r}{\xi L_0} \right)^2 \right] dx = \frac{\pi^2 y_r^2}{8\xi L_0} + \frac{2a_r y_r}{\xi L_0} \quad (8)$$

The work carried out is given as follows:

$$T = N \Delta u_g = \frac{\pi^2 (y_r^2 + 16a_r y_r / \pi^2)}{8\xi L_0} N \quad (9)$$

with the following balance of energy differential

$$\frac{\partial (U_\varepsilon + U_p - T)}{\partial y_r} = \frac{\pi^4 \gamma_J EI_B y_r}{16(\xi L_0)^3} + \frac{\pi}{\xi L_0} M_p^r - \frac{\pi^2 (y_r + 8a_r / \pi^2)}{4\xi L_0} N = 0 \quad (10)$$

$$N = \frac{\pi^2 \gamma_J EI_B}{(2\xi L_0)^2} \frac{y_r}{y_r + 8a_r / \pi^2} + \frac{4M_p^r}{\pi (y_r + 8a_r / \pi^2)} \quad (11)$$

Approximating $8/\pi^2 \approx 1$, the following is obtained:

$$N \approx \frac{\pi^2 \gamma_J EI_B}{(2\xi L_0)^2} \frac{y_r}{y_r + a_r} + \frac{4}{\pi} \frac{M_p^r}{y_r + a_r} \quad (12)$$

Similar calculations can be carried out for the asymmetrical buckling mode shown in Figure 7(b), as follows.

$$U_p = \frac{y_r}{\xi L_0} \frac{\pi - 2\pi\xi + 4\xi}{1 - 2\xi} M_p^r \quad (13)$$

$$T \approx \frac{\pi^2 N}{8\xi(1 - 2\xi)L_0} (y_r^2 + 16a_r y_r / \pi^2) \quad (14)$$

$$N = \frac{\pi^2(1 - 2\xi)\gamma_J EI_B}{(2\xi L_0)^2} \frac{y_r}{y_r + 8a_r / \pi^2} + \frac{4(1 - 2\xi + 4\xi/\pi)}{\pi(y_r + 8a_r / \pi^2)} M_p^r \quad (15)$$

When $\xi = 0.25$, N can be approximated as follows:

$$N \approx \frac{\pi^2(1 - 2\xi)\gamma_J EI_B}{(2\xi L_0)^2} \frac{y_r}{y_r + a_r} + \frac{M_p^r}{y_r + a_r} \quad (16)$$

When $M_p^r = 0$ and $a_r \ll y_r$, Equation (16) turns into Equation (2). As indicated by Equations (12) and (16), the global buckling strength is generally determined by the asymmetrical mode when the ends of the connections are fixed rigidly.

Secondly, considering the normalized rotational stiffness of the gusset plates, $\xi\kappa_{Rg}$ can be defined as follows:

$$\xi\kappa_{Rg} = \frac{K_{Rg}\xi L_0}{\gamma_J EI_B} \tag{17}$$

Additional displacement due to the rotation of the gusset plate (represented by the end spring shown in the detail of Figure 7(a)) is defined as y_{rs} . Given that the deformation because of the connection zone bending, y_{re} , becomes equivalent to y_{rs} when $\xi\kappa_{Rg} = 3$, the strain energy stored in a specific spring can be approximated as follows:

$$U_\varepsilon = \frac{\pi^4 \gamma_J EI_B y_r^2}{32(\xi L_0)^3} \left(\frac{\xi\kappa_{Rg}}{\xi\kappa_{Rg} + 3} \right)^2 \tag{18}$$

The gusset plate spring rotation, $\Delta\theta_s$, plastic hinge rotation, $\Delta\theta_p$, and axial deformation, Δu_g can be expressed as follows:

$$\Delta\theta_s = \frac{y_r}{\xi L_0} \frac{3}{\xi\kappa_{Rg} + 3} \tag{19}$$

$$\Delta\theta_r = \frac{\pi y_r}{2\xi L_0} \frac{\xi\kappa_{Rg}}{\xi\kappa_{Rg} + 3} + \frac{y_r}{\xi L_0} \frac{3}{\xi\kappa_{Rg} + 3} = \frac{y_r}{2\xi L_0} \frac{\pi\xi\kappa_{Rg} + 6}{\xi\kappa_{Rg} + 3} \tag{20}$$

$$\Delta u_g = \frac{y_r^2 + 2a_r y_r}{\xi L_0} \left(\frac{3}{\xi\kappa_{Rg} + 3} + \frac{\pi^2}{8} \frac{\xi\kappa_{Rg}}{\xi\kappa_{Rg} + 3} \right) = \frac{y_r^2 + 2a_r y_r}{\xi L_0} \frac{\pi^2 \xi\kappa_{Rg} + 24/\pi^2}{8(\xi\kappa_{Rg} + 3)} \tag{21}$$

Then, the energy stored in the springs, U_s , energy stored in the hinges, U_p , and the total work done, T , can be evaluated respectively as follows:

$$U_s = \frac{\gamma_J EI_B y_r^2 \xi\kappa_{Rg}}{2(\xi L_0)^3} \left(\frac{3}{\xi\kappa_{Rg} + 3} \right)^2 \tag{22}$$

$$U_p = \frac{y_r}{\xi L_0} \frac{\pi\xi\kappa_{Rg} + 6}{\xi\kappa_{Rg} + 3} M_p^r \tag{23}$$

$$T = \frac{\pi^2 (y_r^2 + 2a_r y_r)}{8\xi L_0} \frac{\xi\kappa_{Rg} + 24/\pi^2}{\xi\kappa_{Rg} + 3} N \tag{24}$$

With the balance of energy differential $\partial(U_\varepsilon + U_s + U_p - T)/\partial y_r = 0$,

$$N \approx \frac{\pi^2 \gamma_J EI_B}{(2\xi L_0)^2} \cdot \frac{\xi\kappa_{Rg}}{\xi\kappa_{Rg} + 24/\pi^2} \cdot \frac{y_r}{y_r + a_r} + \frac{4}{\pi} \cdot \frac{M_p^r}{y_r + a_r} \cdot \frac{\xi\kappa_{Rg} + 6/\pi}{\xi\kappa_{Rg} + 24/\pi^2} \tag{25}$$

Equation (25) may be expressed as Equation (26) when the rotational stiffness of the gusset plates is negligible ($\xi\kappa_{Rg} \approx 0$).

$$N = \frac{M_p^r}{y_r + a_r} \tag{26}$$

Conversely, if $\xi\kappa_{Rg} \rightarrow \infty$, Equation (25) is restored to match Equation (12). Hence, Equation (25) covers the symmetrical buckling strength for rotational stiffness values ranging from those of pinned ends to those of rigid ends.

The asymmetrical collapse mechanism strength can be derived following a similar process (Figure 7(b)) to obtain Equation (27).

$$N \approx \frac{\pi^2(1 - 2\xi)\gamma_J EI_B}{(2\xi L_0)^2} \cdot \frac{\xi \kappa_{Rg}}{\xi \kappa_{Rg} + 24/\pi^2} \cdot \frac{y_r}{y_r + a_r} + \frac{M_p^r}{y_r + a_r} \tag{27}$$

Accordingly, one-sided buckling mode strength, shown in Figure 7(c), can be determined using the following expression.

$$N \approx \frac{\pi^2(1 - 2\xi)\gamma_J EI_B}{(2\xi L_0)^2} \frac{\xi \kappa_{Rg}}{(1 - \xi)(\xi \kappa_{Rg} + 24/\pi^2)} \frac{y_r}{y_r + a_r} + \frac{M_p^r}{y_r + a_r} \tag{28}$$

Similar to Equation (25), Equations (27) and (28) cover asymmetrical or one-sided buckling strength for varying gusset plate rotational stiffness values. Equation (28) yields results similar to those of Okazaki *et al.* [12] for relatively small a_r and y_r values. Equation (27) yields lower values than do Equation (25) or Equation (28), thus implying that the asymmetrical mode governs stability.

Here, if $a_r \ll y_r$, Equation (27) can be approximated as follows:

$$N \approx \frac{\pi^2(1 - 2\xi)\gamma_J EI_B}{(2\xi L_0)^2} \cdot \frac{\xi \kappa_{Rg}}{\xi \kappa_{Rg} + 24/\pi^2} + \frac{M_p^r}{y_r + a_r} = N_{cr}^r + \frac{M_p^r}{y_r + a_r} \tag{29}$$

where N_{cr}^r is the global elastic buckling strength of the connection zone with pinned conditions at the restrainer ends.

Equation (29), which describes the ultimate strength path shown in Figure 6, indicates that the axial force decreases for increasing values of the out-of-plane displacement y_r . As shown in Figure 6, when the elastic axial force and the out-of-plane displacement relationship considering initial imperfections expressed by Equation (3) exceed the limits of the aforementioned possible mechanisms, it is considered that the BRB is expected to start undergoing global buckling. Substituting $y_r = a_r N / (N_{cr}^B - N)$ from Equation (3) into Equation (29), the required restrainer moment transfer capacity, M_p^r , can be approximated as follows:

$$M_p^r = \frac{a_r}{1 - N/N_{cr}^B} [N - N_{cr}^r] \tag{30}$$

When the brace is subjected to an axial force along with an out-of-plane drift, a bending moment is generated as shown in Figure 8. The restrainer moment transfer capacity is considered to be reduced by this secondary moment M_0^r . From Figure 8, this value can be estimated as follows:

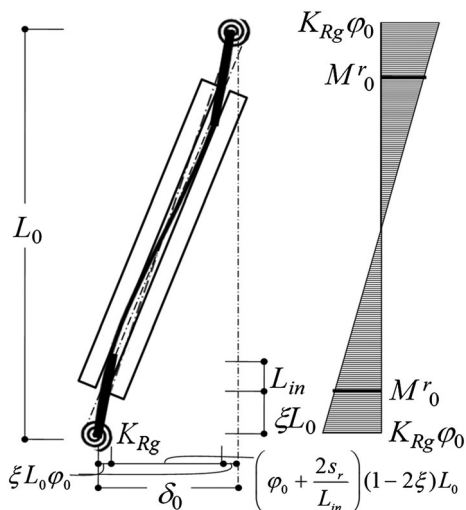


Figure 8. Additional bending moment under out-of-plane drift.

$$M_0^r = (1 - 2\xi)K_{Rg} \left[\frac{\delta_0}{L_0} - \frac{2s_r(1 - 2\xi)}{L_{in}} \right] \geq 0 \tag{31}$$

where δ_0 denotes the assumed maximum story out-of-plane drift, and L_{in} denotes the insert zone length. Including M_0^r in Equation (29), the following equation for defining the ultimate strength is obtained:

$$N = N_{cr}^r + \frac{M_p^r - M_0^r}{y_r + a_r} \tag{32}$$

When the aforementioned N is substituted for the axial force in Equation (30), the stability condition can be expressed as follows:

$$M_p^r - M_0^r \geq \frac{a_r}{1 - N_{cu}/N_{cr}^B} (N_{cu} - N_{cr}^r) \tag{33}$$

where $M_p^r - M_0^r$ should be taken as zero if the difference is negative.

In Equation (33), N_{cr}^B can be estimated by eigenvalue analysis; however, when $\gamma_j \approx 1$, the lowest value decided by the elastic symmetrical mode can be approximated as N_{cr}^B using the following expression:

$$\begin{cases} N_{cr}^B = \frac{4\pi^2 EI_B L \kappa_{Rg}^2 + 10 L \kappa_{Rg} + 16}{L_0^2 L \kappa_{Rg}^2 + 14 L \kappa_{Rg} + 64} \\ L \kappa_{Rg} = K_{Rg} \frac{L_0}{EI_B} \end{cases} \tag{34}$$

where $L \kappa_{Rg}$ is the rotational stiffness of the gusset plate normalized by total length. For satisfying Equation (33), two approaches can be followed.

- (1) When $\varepsilon \kappa_{Rg}$ is sufficiently large, the left part of Equation (33) tends to be small or zero. In order to satisfy Equation (33) N_{cr}^r should be larger than N_{cu} . This approach corresponds to Equation (2), which allows for hinges at the restrainer ends (Figure 2(a)).
- (2) Decrease M_0^r and N_{cr}^r by decreasing $\varepsilon \kappa_{Rg}$ and providing sufficient bending strength M_p^r to satisfy Equation (33). This approach corresponds to transferring the bending moment at the restrainer-end zone (Figure 2(b)).

With the use of these two approaches, Equation (33) covers the two design concepts discussed in Figure 2.

The proposed stability condition in Equation (33) is based on the condition that the gusset plates remain elastic. When plastic hinges are produced at the gusset plates, a different global buckling mode as shown in Figure 9 comes into play. The stability condition for this collapse mode can be expressed as follows.

$$\left[(1 - 2\xi)M_p^s - M_0^r \right] + (M_p^r - M_0^r) \geq \frac{a_r}{1 - N_{cu}/N_{cr}^B} N_{cu} \tag{35}$$

where M_p^s is the plastic bending strength of the gusset plate including the axial force effect, and $(1 - 2\xi)M_p^s - M_0^r$ or $M_p^r - M_0^r$ should be taken as zero if the difference is negative.

3. CYCLIC BRB LOADING TESTS WITH OUT-OF-PLANE DRIFT

For confirming the proposed stability conditions, cyclic loading tests were performed on BRBs with out-of-plane drifts. This test program simulated the worst-case scenario in which the maximum in-plane story drift occurs at the same as the 1% out-of-plane story drift. The test configuration with the specimen is shown in Figures 10 and 11, and the test matrix is summarized in Table I. The core plate material was JIS-SN400B (average yield strength: 270 MPa), and the core cross section size,

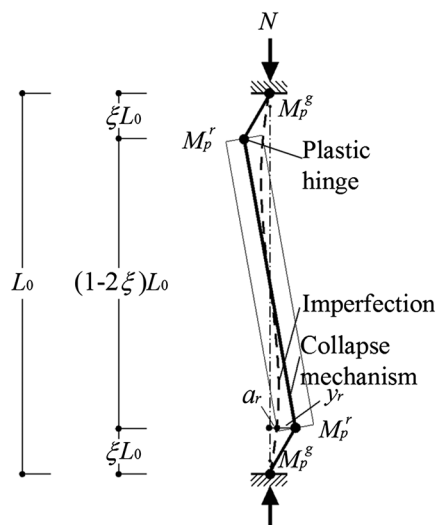


Figure 9. Collapse mechanism with plastic hinges at gusset plate ends.

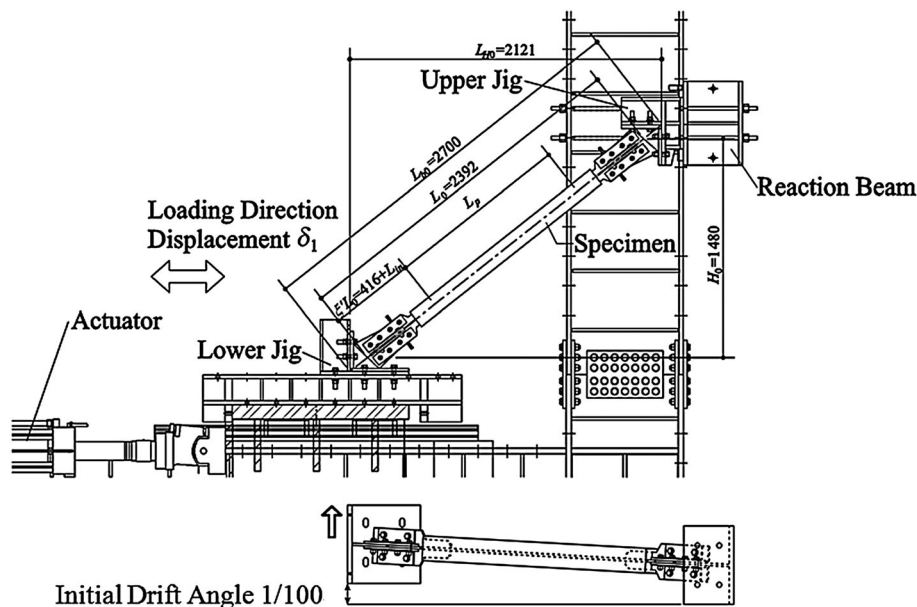


Figure 10. The cyclic loading test setup.

$A_c = 12 \text{ mm} \times 90 \text{ mm}$. The restrainer is either a mortar filled square box section with a side length of 125 mm and thickness of 2.3 mm, or a circular tube with an external diameter of 139.8 mm and tube wall thickness of 3.2 mm. Two types of gusset plates are used in the tests, namely, the regular type ($\xi \kappa_{Rg} = 0.04$) and the stiffened type ($\xi \kappa_{Rg} = 0.3$). The insert length of the stiffened part of the core plate into the restrainer, L_{in} , is chosen to be 90 mm and 180 mm, which are equal to 1.0 and 2.0 times the core plate width, respectively. In addition, the core plate–restrainer clearance varies from 1.0 mm to 2.0 mm. The specimens are labeled as M (R: rectangular, C: circular), L (insert zone length to core plate width ratio), S (clearance), and H (stiffened type gusset plate).

Prior to each test, an out-of-plane displacement equivalent to 1% radian story drift was applied to each specimen. For cyclic loading, up to 3% normalized axial deformation (δ/L_p) was applied, according to the loading protocol shown in Figure 12. Here, the normalized axial deformation, which is approximately equivalent to the story drift angle, is the ratio of the axial deformation to the

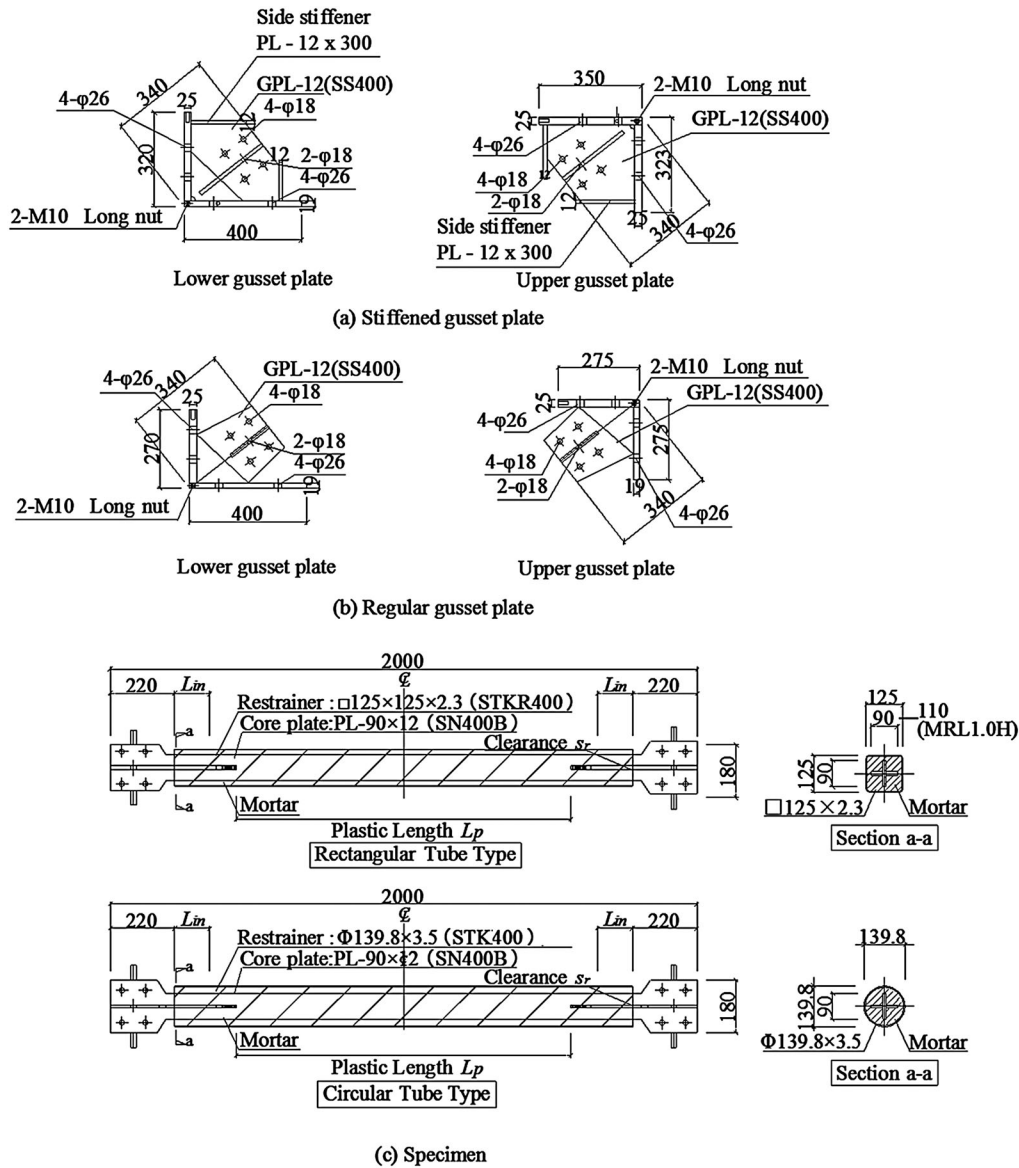


Figure 11. The loading protocol.

plastic length of the core plate L_p . The expected values of the initial imperfection angles for each specimen are summarized in Table II.

The hysteresis loops obtained by cyclic loading tests for each specimen are shown in Figure 13. The normalized cumulative plastic deformation $\Sigma \Delta \epsilon_p = \Sigma \Delta \delta_p / L_p$, and normalized cumulative absorbed energy $\chi_w = E_d / \sigma_y A_c$ until instability are also noted in each figure. Specimen MRL1.0S1H (Figure 12(a)) with stiffened gusset plates showed stable hysteretic behavior until core plate fracture after 6 cycles of over 3.5% (48.3 mm) normalized axial deformation. Similarly, MRL2.0S1 (Figure 12(b)) with regular gusset plates showed stable hysteresis until 12 cycles of 3% (36 mm) normalized axial deformation. This performance is considered satisfactory for energy-dissipating braces. MRL2.0S2 (Figure 12 (c)), which has slightly larger initial imperfection compared with that of MRL2.0S1, showed stable hysteresis until the second cycle at 3% (36 mm) normalized axial deformation, after which out-of-plane instability occurred. MCL2.0S2 (Figure 12(d)), using a mortar filled circular steel tube, showed stable hysteresis until the second cycle at 2% (27.6 mm) normalized axial deformation, at which time out-of-plane instability occurred. MRL1.0S1 (Figure 12(e)) reached the yield strength of the core plate and showed stable hysteresis up to the second cycle of 1.0% (13.8 mm) normalized axial deformation,

Table I. Test matrix.

Specimen	A_c (mm ²)	σ_{cy} (N/mm ²)	EI_B (Nmm)	σ_{ry} (N/mm ²)	K_{Rg} (Nmm)	γEI_B (Nmm)	L_0 (mm)	L_{in} (mm)	L_p (mm)	s_r (mm)	ξL_0 (mm)	$\xi' L_0$ (mm)
MRL1.0S1H	1080	266.0	5.81×10^{11}	305.0	6.90×10^8	1.20×10^{12}	2392	90	1380	1	416	506
MRL2.0S1	1080	266.8	5.81×10^{11}	385.8	9.73×10^7	1.20×10^{12}	2392	180	1200	1	416	596
MRL2.0S2	1080	266.8	5.81×10^{11}	391.5	9.73×10^7	1.20×10^{12}	2392	180	1200	2	416	596
MCL2.0S2	1080	269.7	7.14×10^{11}	365.7	9.73×10^7	1.20×10^{12}	2392	180	1200	2	416	596
MRL1.0S1	1080	266.8	5.81×10^{11}	391.5	9.73×10^7	1.20×10^{12}	2392	90	1380	1	416	506
MRL1.0S2	1080	266.8	5.81×10^{11}	391.5	9.73×10^7	1.20×10^{12}	2392	90	1380	2	416	506

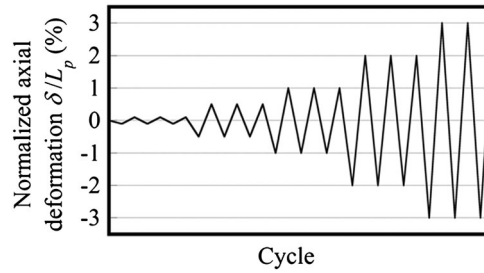


Figure 12. The loading protocol.

Table II. Initial imperfection angle.

Specimen	L_{in} (mm)	s_r (mm)	$\theta_0 = 2s_r/L_{in}$ (rad)
MRL1.0S1H	90	1	0.02
MRL2.0S1	180	1	0.01
MRL2.0S2	180	2	0.02
MCL2.0S2	180	2	0.02
MRL1.0S1	90	1	0.02
MRL1.0S2	90	2	0.04

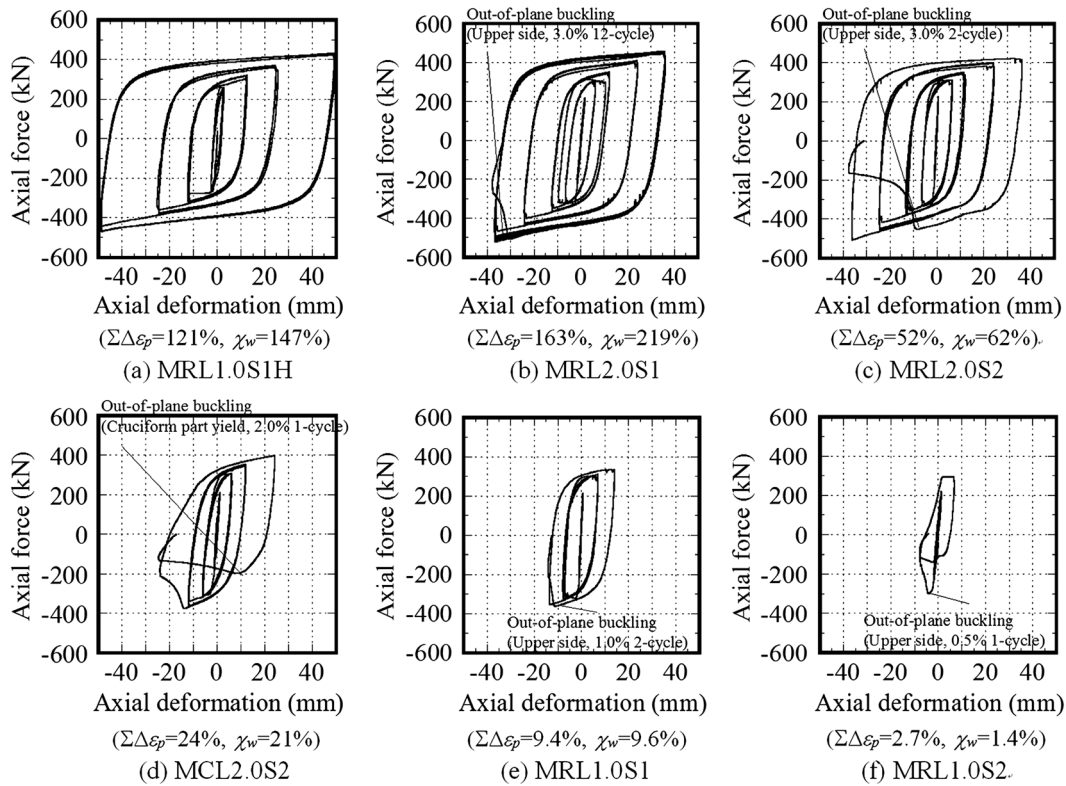


Figure 13. Axial force-deformation relationship.

after which it experienced global buckling associated with hinging at the neck. MRL1.0S2 (Figure 12(f)) showed stable a hysteresis loop for only one cycle of 0.5% (6.9 mm) normalized axial deformation, then experienced axial global buckling associated with hinging at the neck.

These test results indicate that BRB stability is significantly affected by the length of the insert zone and the clearance, as is expected from the proposed Equations (33) and (35). In order to confirm the validity of the proposed equations, each specimen is evaluated using Equations (33) and (35). To this end, restrainer moment transfer capacity M_p^r , of each specimen was estimated using the following equation proposed by Matsui *et al.* [17]:

$$M_p^r = \min \left\{ M_p^{r-neck}, M_p^{r-rest} \right\} \quad (36)$$

where M_p^{r-neck} represents the restrainer moment transfer capacity determined by the cruciform core plate at the neck as follows:

$$M_p^{r-neck} = \left\{ 1 - \left(\frac{N_{cu} - N_{wy}^c}{N_u^c - N_{wy}^c} \right)^2 \right\} Z_{cp} \sigma_{cy} \quad (37)$$

where N_{wy}^c denotes the yield axial force of the cruciform core plate at the web zone, N_u^c denotes the ultimate strength of the cruciform core plate at the neck, Z_{cp} denotes the plastic section modulus at the neck, and σ_{cy} denotes the yield stress of the core plate. In Equation (36), M_p^{r-rest} represents the restrainer moment transfer capacity determined by the restrainer section at rib end as follows:

$$M_p^{r-rest} = \begin{cases} \min \left\{ Z_{rp} \sigma_{ry}, \alpha_p^r [K_{Rr1} \theta_{y1}' + K_{R2} (\theta_{y2} - \theta_{y1}')] \right\} & \text{(Rectangular Tube)} \\ \min \left\{ Z_{rp} \sigma_{ry}, \alpha_p^r K_{Rr1} \theta_y \right\} & \text{(Circular Tube)} \end{cases} \quad (38)$$

$$\alpha_p^r = 4.5 - 1.5(L_{in}/B_c) \quad (0.5 \leq L_{in}/B_c < 2)$$

where Z_{rp} denotes the plastic section modulus of the restrainer tube, σ_{ry} denotes restrainer yield stress, K_{Rr1} denotes the restrainer elastic rotational stiffness about the rib end, θ_{y1}' denotes the pseudo initial yield angle of the rectangular restraint tube, K_{R2} denotes the post-yielding rotational stiffness of the restrainer about the rib end, θ_{y2} denotes the angle at which the plastic hinge occurs, θ_y denotes the yield angle of the circular restraint tube, and B_c denotes the core plate width.

In most cases, M_p^r is determined by the bending strength of the neck section, M_p^{r-neck} , given by Equation (37) when the insert zone length is more than 2.0 times the core plate width. The obtained values of M_p^r for each specimen are summarized in Table III. The expected failure axial force assuming elastic springs for gusset plates N_{lim1} is obtained by solving Equation (39), which is derived from Equation (33) and summarized in Table. IV.

$$N_{lim1} = \frac{(M_p^r - M_0^r)/a_r + N_{cr}^r}{(M_p^r - M_0^r)/(a_r N_{cr}^B) + 1} > N_{cu} \quad (39)$$

Table III. Bending capacities at restrainer ends.

Specimen	Yield bending strength of cruciform zone (kNm)	Yield bending strength of restrainer (kNm)	M_p^r (kNm)
MRL1.0S1H	2.46	2.97	2.46
MRL2.0S1	5.50	8.38	5.50
MRL2.0S2	6.56	8.56	6.56
MCL2.0S2	6.50	35.68	6.50
MRL1.0S1	6.78	4.28	4.28
MRL1.0S2	6.78	4.28	4.28

Table IV. Stability evaluations using proposed equation.

Specimen	N_{cr}^B (kN)	a_r (mm)	N_{cr} (kN)	N_{cr} (kN)	M_o (kNm)	Failure cycle at experiment	Stability limit (kN)		Failure axial force in experiment (kN)
							N_{lim1} (Equation (39))	N_{lim2} (Equation (41))	
MRL1.0S1H	1880	11.4	695	431	0.00	None	818	1390	(452)
MRL2.0S1	1158	6.80	82	432	0.09	3.0%-12cycle	520	520	535
MRL2.0S2	1158	12.4	82	432	0.00	3.0%-2cycle	419	410	507
MCL2.0S2	1389	12.4	82	437	0.00	1.0%-2cycle	440	432	375
MRL1.0S1	1158	11.4	111	432	0.00	0.5%-1cycle	367	345	362
MRL1.0S2	1158	21.7	111	432	0.00	0.5%-1cycle	264	217	300

* N_{cr} is estimated as $1.5A_c\sigma_{cy}$ (approximately equivalent to axial forces of the first 3% normalized axial deformation).
 (): Exceptionally, MRL1.0S1H did not fail, so only the maximum applied axial force is shown above.

Here, N_{cr}^r is estimated as the elasto-plastic buckling strength obtained by substituting the equivalent slenderness ratio of Equation (40) into the column curves. In Equation (40), ζ' from Figure 4 instead of ζ should be used for assuming whether plastic hinges can be produced at the rib ends.

$$\lambda_r = \frac{2\zeta' L_0}{i_c} \cdot \sqrt{\frac{\xi \kappa_{Rg} + 24/\pi^2}{(1 - 2\zeta') \xi \kappa_{Rg}}} \tag{40}$$

where i_c is the radius of gyration at the connection zone.

Similarly, the expected failure axial force that assumes plastic hinges at the gusset plates, N_{lim2} , is determined by solving Equation (41), which is derived from Equation (35).

$$N_{lim2} = \frac{\left[(1 - 2\zeta) M_p^g + M_p^r - 2M_0^r \right] / a_r}{\left[(1 - 2\zeta) M_p^g + M_p^r - 2M_0^r \right] / (a_r N_{cr}^B) + 1} > N_{cu} \tag{41}$$

The least of the two failure forces obtained from Equations (39) and (41) is considered the failure axial force of the specimen. In Table IV, the estimated N_{lim1} and N_{lim2} values are compared with the maximum axial loads in the experiments. It is shown that the stability limit of specimens MRL1.0S1H and MRL2.0S1 exceed the expected N_{cu} (assumed as $N_{cu} = 1.5 \times A_c \times \sigma_{cy}$). The other specimens were designed such that the stability limit failed to exceed the N_{cu} , thus indicating that their global stability is not guaranteed. Figure 14 shows a comparison of the measured axial force–displacement relationships with those obtained using Equations (3) and (32). In the figure, the ultimate strength paths for the collapse mechanisms are given by R1, C1, R2, and C2. Here R stands for rib end, C stands for the neck cruciform section; 1 and 2 stand for N_{lim1} or N_{lim2} failure axial forces, respectively. Although the test results that exceeded the stability limit have better force–displacement relationships compared with those obtained using the proposed equations, their paths tend to be parallel to the estimated collapse path.

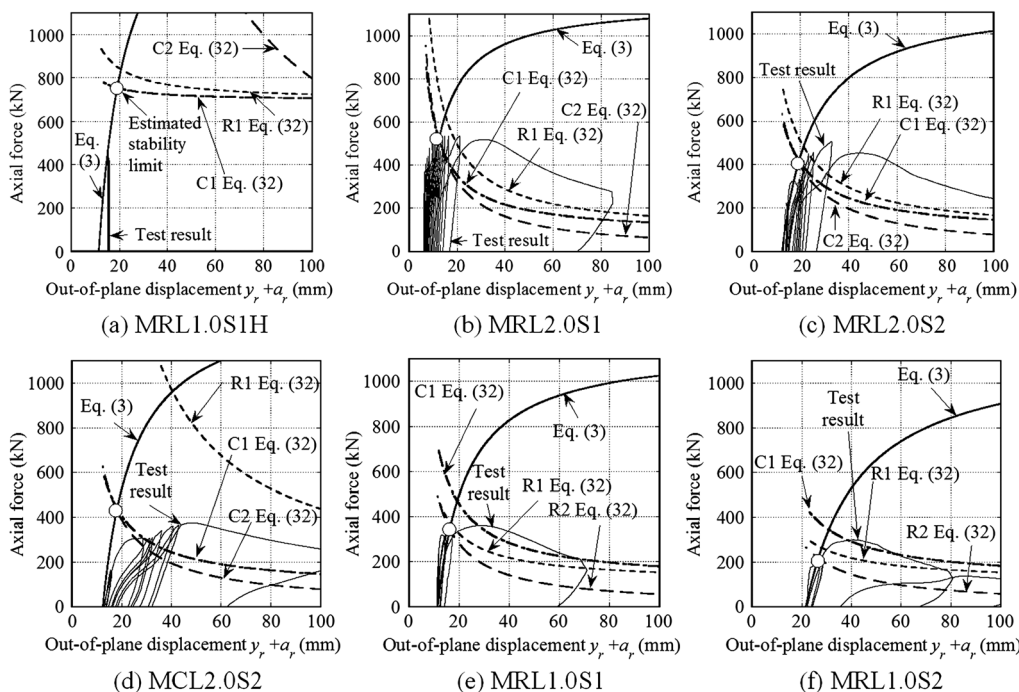


Figure 14. Axial force versus out-of-plane displacement relationship.

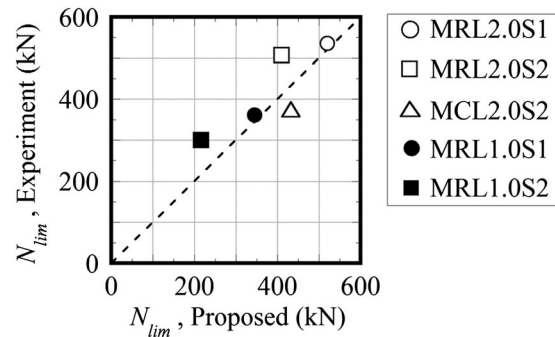


Figure 15. Distribution of proposed/experimental accuracy by specimen type.

A comparison of the estimated failure axial forces N_{lim} , which is the smaller of N_{lim1} and N_{lim2} , with the peak axial force from experimental results, is shown in Figure 15. It can be seen that the results of the proposed equations are consistent with the experimental results with some variation. In general, the given safety condition successfully estimates the performance of each test specimen and is therefore considered valid.

4. CONCLUSIONS

When BRBs exhibit global buckling behavior, a certain amount of bending moment is transferred between the core section and restrainer tube end, which is defined as restrainer moment transfer capacity in this study. The restrainer moment transfer capacity depends on the internal structure of the BRB, as explained throughout the paper, and significantly influences BRB stability. This study proposes a compact set of equations for evaluating global BRB stability considering restrainer moment transfer capacity. The proposed equations cover a wide range of BRB connections from rigid end to pinned end.

Cyclic loading tests were performed on full-scale BRBs with initial out-of-plane drifts and varying connection stiffness values to confirm the proposed stability conditions and validating the proposed equations. The conclusions of this study are as follows:

- (1) The BRB stability conditions were expressed by a set of simple equations as functions of restrainer moment transfer capacity, rotational stiffness at gusset plate ends, initial imperfections governed by core-plate clearances, and expected out-of-plane story drifts. This equation set covers the stability conditions of all BRB types regardless of the gusset plate rigidity or restrainer moment transfer capacity.
- (2) In the cyclic loading tests with initial out-of-plane drifts, specimens with shorter insert zones and larger clearances experienced global buckling before achieving stable hysteresis, whereas specimens with longer insert zones and smaller clearances showed more stable hysteresis, which may be attributed to the fact that the restrainer moment transfer capacity significantly influences BRB stability.

In addition, the specimens with stiffened gusset plates exhibited greater stable hysteresis and higher axial capacity even with shorter insert zones. These results agree with the stability conditions anticipated using the proposed stability equations.

- (3) The proposed equation set can be applied for directly evaluating the stability limit strength of BRBs. The results have shown that the evaluated stability limit strengths agree well with the experimental results of buckled specimens, thus validating the proposed equations.

Stability conditions for different types of BRBs such as pin-connected BRBs or ones with alternative restrainer shapes will be discussed in future papers, the studies corresponding to which are in progress.

ACKNOWLEDGEMENTS

The authors would like to acknowledge the support of Nippon Steel and Sumikin Engineering Co. Ltd for this study.

NOTATIONS

a :	maximum imperfection along the restrainer
a_r :	total initial imperfection
e :	axial force eccentricity
i_c :	radius of gyration at connection zone
l_B :	restrained zone length
s_r :	clearance between core and restrainer
y_r :	out-of-plane deformation at restrainer end
y_{re} :	additional out-of-plane deformation due to connection zone bending
y_{rs} :	additional deformation due to end spring rotation
A_c :	core plate cross section
B_c :	core plate width
EI_B :	bending stiffness of restrainer
E_d :	absorbed hysteretic energy until instability or fracture
K_{Rg} :	rotational spring stiffness at gusset plate
K_{Rr1} :	elastic rotational stiffness of restrainer about rib end
K_{Rr2} :	post-yielding rotational stiffness of restrainer about rib end
L_{in} :	insert zone length
L_p :	plastic zone length of core plate
M_0^r :	additional bending moment derived from story out-of-plane drift
M_y^B :	bending strength of restrainer
M_y^g :	plastic bending strength of gusset plate including axial force effect
M_p^r :	restrainer moment transfer capacity
M_p^{r-neck} :	restrainer moment transfer capacity determined by cruciform core plate at neck
M_p^{r-rest} :	restrainer moment transfer capacity determined by restrainer section at rib end
N :	axial force
N_{cu} :	maximum axial strength of core plate
N_{cr}^B :	global elastic buckling strength of BRB including effect of gusset plate rotational stiffness
N_{cr}^r :	global elastic buckling strength with pin conditions at restrainer ends
N_{cr}^R :	Euler buckling strength of restrainer
N_{lim1} :	expected failure force assuming elastic gusset plates
N_{lim2} :	expected failure force assuming plastic hinges at gusset plates
N_u^c :	ultimate axial strength of cruciform core plate at neck
N_{wy}^c :	yield axial force of cruciform core plate at web zone
N_y :	yield axial force of core plate
T :	external work
U_p :	plastic strain energy stored in plastic hinges
U_s :	energy stored in springs
U_e :	strain energy stored in both connection zones
Z_{cp} :	plastic section modulus at neck
Z_{rp} :	plastic section modulus of restrainer tube
$\gamma_J EI_B$:	bending stiffness of connection zone
δ_0 :	story out-of-plane drift
δ :	axial deformation of BRB
δ_p :	axial plastic deformation of BRB
ξL_0 :	connection zone length
$\xi' L_0$:	length between gusset plate end and rib end (= $\xi L_0 + L_{in}$)

$\Delta\theta_r$:	rotational angle of plastic hinge at restrainer end
$\Delta\theta_s$:	rotation at gusset plate
Δu_g :	axial deformation caused by global buckling
χ_w :	normalized cumulative absorbed energy ($=\Sigma\Delta\delta_p/L_p$)
ϕ_0 :	rotational angle at gusset plate due to out-of-plane drift
${}^e\kappa_{Rg}$:	normalized rotational stiffness for gusset plate
${}^L\kappa_{Rg}$:	normalized rotational stiffness for gusset plate by total length
λ_r :	equivalent slenderness ratio for global elastic buckling strength with pin conditions at restrainer ends
θ_0 :	initial imperfection angle of connection zone
θ_y :	yield angle for circular restrainer tube
θ'_{y1} :	pseudo initial yield angle for rectangular restrainer tube
θ_{y2} :	angle at which plastic hinge occurs at restrainer end
$\Sigma\Delta\varepsilon_p$:	normalized cumulative plastic deformation ($=E_d/\sigma_y A_c$)
σ_{cy} :	yield stress of core plate material
σ_{ry} :	yield stress of restrainer tube material

REFERENCES

1. Architectural Institute of Japan: Recommendations for stability design of steel structures, Sec. 3.5 Buckling-Restrained Braces, 2009, 74–79.
2. AISC341-10: Seismic provisions for structural steel buildings, 2010, F4: Buckling-Restrained Braced Frames.
3. Takeuchi T, Ida M, Yamada S, Suzuki K. Estimation of cumulative deformation capacity of buckling restrained braces. *ASCE Journal of Structural Engineering* 2008; **134**(5):822–831.
4. Takeuchi T, Hajjar JF, Matsui R, Nishimoto K, Aiken ID. Local buckling restraint condition for core plates in buckling restrained braces. *Journal of Constructional Steel Research* 2010; **66**:139–149.
5. Tsai JC, Hsiao PC. Pseudo-dynamic test of a full-scale CFT/BRB frame-Part II: seismic performance of buckling-restrained braces and connections. *Journal of Earthquake Engineering and Structural Dynamics* 2008; **37**:1099–1115.
6. Lin PC, Wang KJ, Yu YJ, Wei CY, Wu AC, Tsai CY, Lin CH, Chen JC, Schellenberg AH, Mahin SA, Roeder CW. Seismic design and hybrid tests of a full-scale three-story buckling-restrained braced frame using welded end connections and thin profile. *Journal of Earthquake Engineering and Structural Dynamics* 2012; **41**:1001–1020.
7. Wigle VR, Fahnestock LA. Buckling-restrained braced frame connection performance, *Journal of Constructional Steel Research* 2010; **66**:65–74.
8. Koetaka Y, Kinoshita T, Inoue K, Iltani K. Criteria of buckling-restrained braces to prevent out-of-plane buckling, *Proceedings of 14th World Conference on Earthquake Engineering*, 2008.
9. Zhao J, Wu B, Ou J. A novel type of angle steel buckling-restrained brace: cyclic behavior and failure mechanism. *Journal of Earthquake Engineering and Structural Dynamics* 2011; **40**:1083–1102.
10. Zhao J, Wu B, Ou J. Flexural demand on pin-connected buckling-restrained braces and design recommendations. *ASCE Journal of Structural Engineering* 2011; **138**(11):1398–1415.
11. Hikino T, Okazaki T, Kajiwara K, Nakashima M. Out-of-plane stability of buckling-restrained braces, *Proceedings of ASCE Structural Congress*, 2011.
12. Okazaki T, Hikino T, Kajiwara K. Out-of-plane stability of buckling-restrained braces, *Proceeding of 15th World Conference on Earthquake Engineering*, 2012.
13. Chou CC, Chen PJ. Compressive behavior of central gusset plate connections for a buckling-restrained braced frame. *Journal of Constructional Steel Research* 2009; **65**:1138–1148.
14. Chou CC, Liu JH, Pham DH. Steel buckling-restrained braced frames with single and dual corner gusset connections: seismic tests and analyses, *Journal of Earthquake Engineering and Structural Dynamics* 2012; **41**:1137–1156.
15. Eryasar ME, Topkaya C. An experimental study on steel-encased buckling-restrained brace hysteretic dampers. *Journal of Earthquake Engineering and Structural Dynamics* 2010; **39**:561–581.
16. Ji X, Hikino T, Kasai K, Nakashima M. Damping identification of full-scale passively controlled five-story steel building structure. *Journal of Earthquake Engineering and Structural Dynamics* 2013; **42**:277–295.
17. Matsui R, Takeuchi T, Nishimoto K, Takahashi S, Ohyama T. Effective buckling length of buckling restrained braces considering rotational stiffness at restrainer ends, *7th International Conference on Urban Earthquake Engineering & 5th International Conference on Earthquake Engineering Proceedings*, 2010; 1049–1058.